IEEE Access
Multidisciplinary : Rapid Review : Open Access Journal

Received March 18, 2019, accepted April 28, 2019, date of publication May 7, 2019, date of current version May 20, 2019.

Digital Object Identifier 10.1109/ACCESS.2019.2915236

Circularly Polarized Annular Ring Antenna With Wide Axial-Ratio Bandwidth for Biomedical Applications

LI-JIE XU[1], YAMING BO[1], (Member, IEEE), WEN-JUN LU[2], (Member, IEEE), LEI ZHU[1,3], (Fellow, IEEE), AND CHENG-FEI GUO[4]

[1]National and Local Joint Engineering Laboratory of RF Integration and Micro-Assembly Technology, Nanjing University of Posts and Telecommunications, Nanjing 210023, China
[2]Jiangsu Key Laboratory of Wireless Communications, Nanjing University of Posts and Telecommunications, Nanjing 210003, China
[3]Department of Electrical and Computer Engineering, Faculty of Science and Technology, University of Macau, Macau 999078, China
[4]College of Telecommunications and Information Engineering, Nanjing University of Posts and Telecommunications, Nanjing 210023, China

Corresponding author: Lei Zhu (leizhu@umac.mo)

This work was supported in part by the National Natural Science Foundation of China under Grant 61601241 and Grant 61871233, in part by the Natural Science Foundation of Jiangsu Province under Grant BK20160917, in part by the Nanjing University of Posts and Telecommunications Startup Foundation (NUPTSF) under Grant NY217002, and in part by the Open Research Fund of the National and Local Joint Engineering Laboratory of RF Integration and Micro-Assembly Technology under Grant KFJJ20180102.

ABSTRACT This paper proposes a novel circularly polarized antenna operating at 2.4–2.48-GHz industrial, scientific, and medical (ISM) band for biomedical applications. This proposed structure is developed from a simple pin-loaded patch antenna, whose circular polarization (CP) is mainly attributed to the loading of shorting pins and L-shaped open-end slot. Based on this, pin-loaded annular ring (PLAR) with dual-mode operation is adapted to introduce another resonance. In addition, two closely coupled rectangular patches are added to bring these two resonant frequencies close to each other in muscle. Furthermore, by introducing arc-shaped slots, CP property and improved impedance matching are achieved with size miniaturization. This proposed structure shows a simulated impedance bandwidth of 8% and a wide axial-ratio (AR) bandwidth of 19.1%. Finally, measurement is performed for the proposed antenna, and the results coincide well with the simulation ones, indicating that it is a good candidate for biomedical applications.

INDEX TERMS Biomedical application, circular polarization, implantable antenna, pin-loaded annular ring.

I. INTRODUCTION

With the collaboration of biomedicine and telecommunication industry, antennas implanted into human body have attracted more and more attentions due to the convenience brought for diagnosing and treating human diseases. These implantable antennas, intended for transmitting physiological data, are normally embedded in human body through surgery or swallowed into digestive tract.

Many groups have devoted to doing research on implantable antennas. Some early works [1]–[10] of implantable antenna presented preliminary design guidelines, brought up a few challenges in design, and demonstrated the feasibility of several suitable structures, such as planar inverted-F antennas [1]–[5], dipoles [6], [7] and cavity slot antenna [8]. The research work on implantable antenna in [1] proposed six-layer spherical model for human head imitation, and simplified one-layer and three-layer models for human chest imitation. For [2] and [9], mimicking gels were developed at medical implant communications service (MICS) (402–405 MHz) and industrial, scientific, and medical (ISM) (2.4–2.48 GHz) band based on the electrical properties of skin. Furthermore, the effects of insulating layers on the performance of implantable antenna were analyzed [10]. Then some follow-up works from various groups did further research on miniaturization, dual-band and wideband operation, biocompatibility and specific absorption rate (SAR) restriction of implantable antenna [11]–[18]. However, these works mentioned above mainly focused on the design of linear polarized implantable antennas.

While in actual applications, due to the invisibility of implants inside human body, it is difficult to precisely detect the orientation of implantable antenna, which raises a problem of how to place the receiving antenna. Thus, circular

The associate editor coordinating the review of this manuscript and approving it for publication was Chow-Yen-Desmond Sim.

polarization (CP) is definitely preferred for implantable antenna to establish effective and efficient communication between in-body implants and out-of-body stations.

CP properties have been studied in different implantable antenna structures during recent years, and patch structure is commonly adopted. For example, by inserting a cross-shaped slot with unequal-length arms in the ground plane of a truncated patch antenna, implantable antenna with CP performance was realized and its 3-dB axial-ratio (AR) bandwidth is 6.09% [19]. In [20], CP antenna was obtained with compact size and wide beamwidth by employing four C-shaped slots and a complementary split-ring resonator. In [21], an annular-ring antenna with CP performance was presented for implantable application. Besides, C. R. Liu etc. proposed several implantable CP antennas based on patch structure [22]–[24], loaded with either slots or stubs, and good miniaturization is achieved. However, the patch antennas mentioned above all have limited axial-ratio (AR) bandwidth, which need further improvement. Other structures like helical and conformal antennas [25], [26] were studied. But their specific structure and high profile limit their application in capsules.

Recently, shorting pins were introduced into implantable antenna design to achieve wide AR bandwidth while maintaining low profile. The typical works include our previous antenna with two shorting pins, the miniaturization principle of which is explained by the slow-wave concept [27]. And then a follow-up work which adopts three pins and open-end slots is introduced [28]. Both these two implantable antennas with loaded pins have a wide AR bandwidth and compact size. However, both of them have not given a detailed explanation of the working principle on CP property.

Therefore, in this paper, we propose a low-profile annular ring antenna with a compact size of $\pi \times 5^2 \times 1.27$ mm^3 at 2.4 – 2.48 GHz ISM band for biomedical applications. With two shorting pins loaded on an annular ring, even and odd mode can be split, giving rise to wide impedance bandwidth. Furthermore, two arc-shaped open-end slots are introduced symmetrically around the center, resulting in wide AR bandwidth. The working principle of CP performance for the proposed antenna is explained specifically by employing a simplified pin-loaded patch antenna. Finally, the predicted and simulated performances of the proposed antenna are verified by measurement, which evidently reveals that the proposed antenna can attain satisfactory CP performance for implantable applications.

II. PIN LOADED IMPLANTABLE PATCH ANTENNA WITH CP PROPERTY

For biomedical applications, an implantable antenna needs to be embedded in human body during data transmission, and muscle tissue is adopted in simulation. As shown in Fig. 1, the antenna is placed into a muscle box whose size is 60 mm × 60 mm ×60 mm with an embedded depth of h = 3 mm, which is the simulation environment throughout this paper if not specified otherwise. In design of the implantable antenna, Roger 3010 ($\varepsilon_r = 10.2$, $\tan\delta = 0.0035$) with thickness of 0.635 mm is used as substrate as well as superstrate.

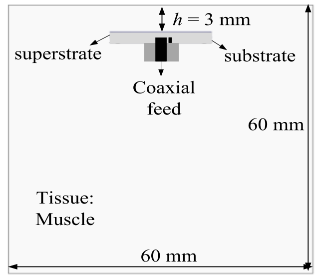

FIGURE 1. Simulation environment for modeling implantable antenna.

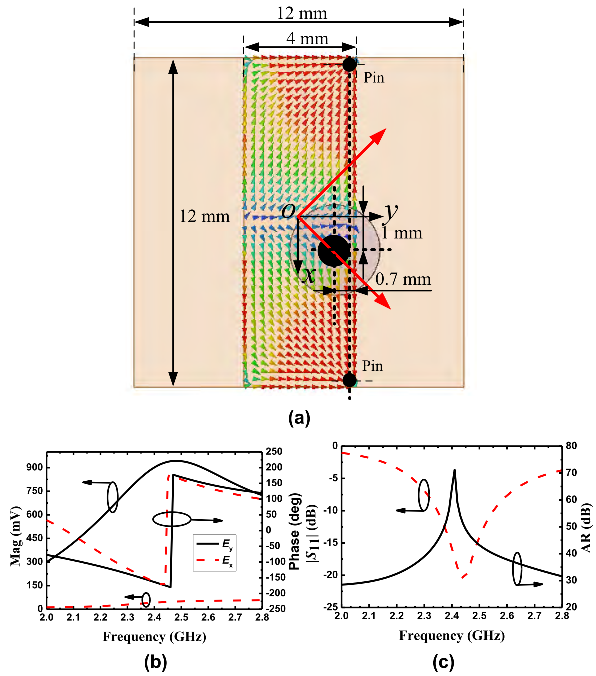

FIGURE 2. (a) Surface current distributions on the pin-loaded patch at 2.44 GHz. (b) The magnitudes and phases of E_x and E_y at boresight. (c) The simulated $|S_{11}|$ and AR at boresight.

As shown in Fig. 2(a), a simple patch antenna is proposed for implantable applications and its dimensions are also labeled in the figure, which are tuned to achieve resonance at 2.45 GHz ISM band. Two symmetric shorting pins are loaded on the patch, leading to strong currents flowing into (or out of) two shorting pins at resonant frequency. It is found that the current distributions are symmetric with respect to y axis, and the currents on upper and lower half patches can be regarded as two currents of same magnitude and same phase as denoted in the figure. In this case, the current components along x axis cancel out, resulting an equivalent current mainly flowing along y axis. To analyze the specifics of polarization, the magnitudes and phases of E_x and E_y are simulated as shown in Fig. 2(b). It can be found that the magnitude of E_y is much larger than that of E_x, and the phases of E_x and E_y are essentially the same, which is in correspondence with the analysis above. Fig. 2(c) gives the simulated $|S_{11}|$ and AR, showing that the pin-loaded patch antenna resonates at 2.44 GHz with linear polarization at boresight.

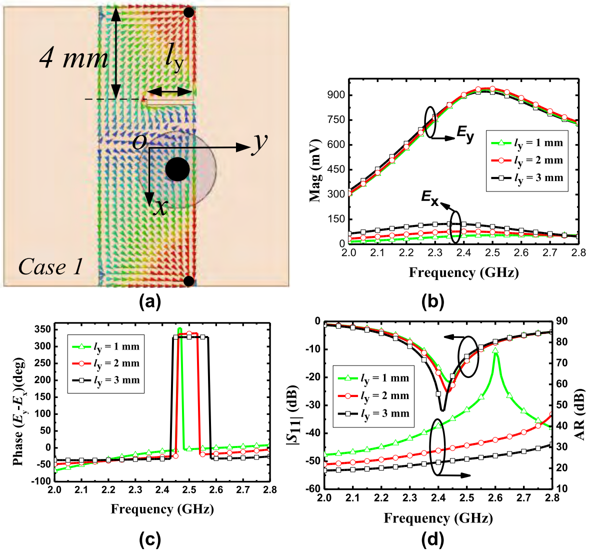

FIGURE 3. **(a) Surface current distributions of proposed cases at resonant frequency. (b) The magnitudes of E_x and E_y varied with l_y. (c) The phase differences between E_y andE_y varied with l_y. (d) The simulated $|S_{11}|$ and AR varied with l_y.**

To obtain CP property, open-end slot is introduced, raising two different cases for discussion. For *case 1* in Fig. 3, only the slot along *y* axis is introduced. And it can be seen from Fig. 3(a) that the strong current on upper half patch is disturbed by the slot, causing asymmetry of the currents between upper and lower half patches. As a result, the current components along *x* axis no longer cancel out, leading to the increasing of magnitude of E_x with the increasing of l_y as can be observed in Fig. 3(b). Meanwhile, the phase difference between E_x and E_y is decreased correspondingly as shown in Fig. 3(c), leading to a gradually lowered AR value as shown in Fig. 3(d). However, the AR value is still above 3 dB.

To achieve better CP performance, *case 2* is developed with the slot length further increased. As depicted in Fig. 4(a), the slot is bended along *x* axis with l_y set to be 3 mm. With the increasing of l_x, the magnitudes of E_x increases whereas that of E_y drops significantly, reaching value equality at 2.49 GHz when $l_x = 7.5$ mm as shown in Fig. 4(b). At the same time, the phase difference between E_x and E_y is further decreased and reaches around 270 deg as can be noted in Fig. 4(c). Correspondingly, the AR value gradually decreases and reaches around 0 dB as shown in Fig. 4(d). Additionally, since the phase of E_y falls around 90 deg behind that of E_x at 2.44 GHz (when $l_y = 3$ mm and $l_x = 7.5$ mm), right-handed circular polarization (RHCP) performance of the simplified pin-loaded patch antenna is achieved. This can also be validated by the simulated surface current distributions as shown in Fig. 5, from which we can see that the predominant transient current rotates anticlockwise in a time period, leading to RHCP performance.

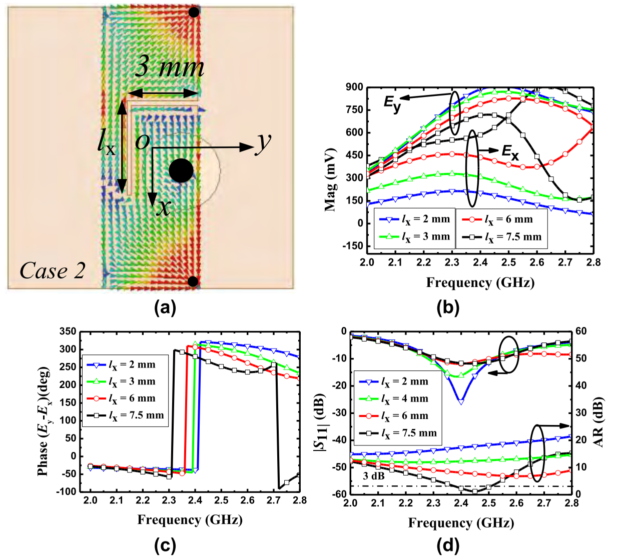

FIGURE 4. **(a) Surface current distributions of proposed cases at resonant frequency. (b) The magnitudes of E_x and E_y varied with l_x. (c) The phase differences between E_y and E_y varied with l_x. (d) The simulated $|S_{11}|$ and AR varied with l_x.**

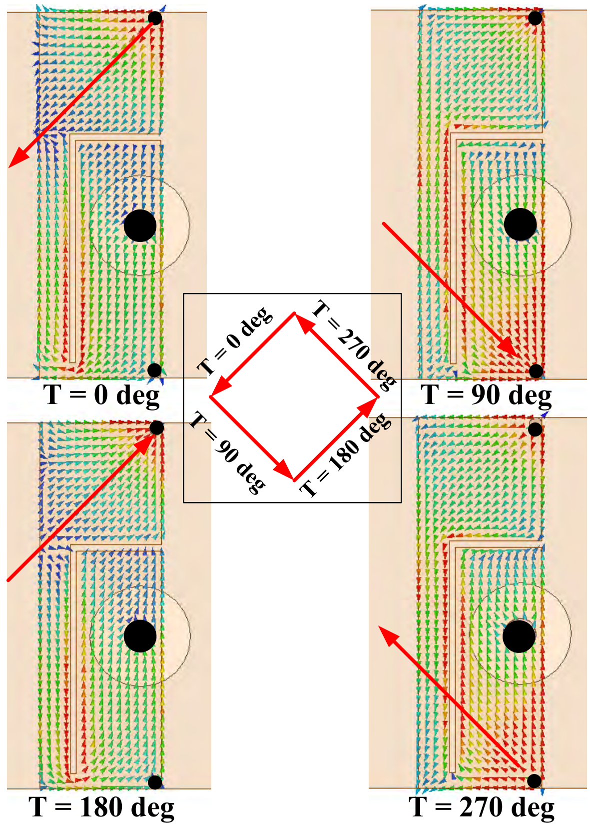

FIGURE 5. **Surface current distributions on pin-loaded patch at 2.45 GHz in a period of T.**

III. PIN-LOADED ANNULAR RING ANTENNA WITH CP PROPERTY

A. PIN-LOADED ANNULAR RING (PLAR) RESONATOR IN AIR

Since only one well-matched resonance is observed for the pin-loaded patch antenna as discussed above,

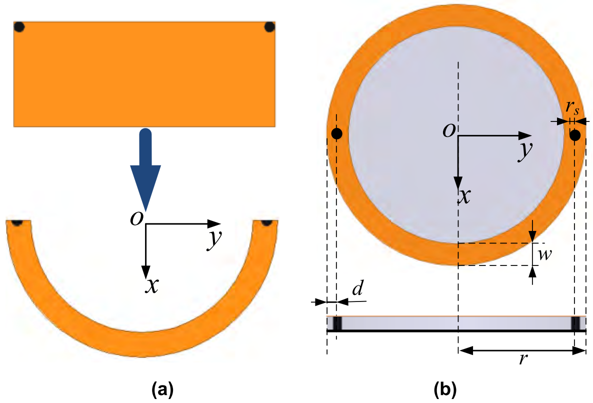

FIGURE 6. (a) Pin-loaded patch bended into semi-circular shape. (b) Geometry of the proposed pin-loaded annular ring (PLAR).

PLAR resonator is adopted as a modification, in which another resonance can be introduced for impedance bandwidth enhancement. As illustrated in Fig. 6, by bending pin-loaded patch antenna, semi-circular pin-loaded patch can be obtained as shown in Fig. 6(a), which corresponds to half of PLAR in Fig. 6(b). Obviously, the semi-circular pin-loaded patch has the same electric field distribution with half of PLAR working at its even mode. And when the even and odd modes of PLAR are excited simultaneously, wider impedance bandwidth can be achieved compared to the simple pin-loaded patch.

Besides, the PLAR is employed as the initial prototype of the implantable CP antennas due to its low profile, small size, and easy fabrication. Also, the smooth profile of its circular shape would cause less discomfort to human body. As shown in Fig. 6(b), The PLAR has a ring width of w and an outer radius of r, which is exactly equal to the radius of ground plane. Two shorting pins are symmetrically loaded on the ring at a distance of d away from the outer edge, connecting the ring with ground.

As we all know, the dominant mode for a ring resonator is TM_{11} mode, and its resonant frequency can be derived as [29]

$$f_{TM_{11}} = \frac{c}{\pi\sqrt{\varepsilon_r}} \cdot \frac{1}{2r - w} \tag{1}$$

where c is the velocity of light and ε_r is the effective relative permittivity. From (1), we can figure out the f_{TM11} is determined by r and w, and the circumference of the annular ring equals to one guided wavelength at resonant frequency.

When two shorting pins are loaded on the annular ring, two resonances corresponding to even and odd modes are excited simultaneously. The extra inductance introduced by two shorting pins mainly contributes to the resonance of even mode, termed as f_1. As for the resonance of odd mode, it is similar to the TM_{11} mode of annular ring, termed as f_2. When operating in air, it is noted that f_1 and f_2 are quite close when w and d are relatively small. To better illustrate this phenomenon, f_1 and f_2 varying with w are given in Fig. 7, where r and r_s are selected as 7 mm and 0.2 mm, respectively.

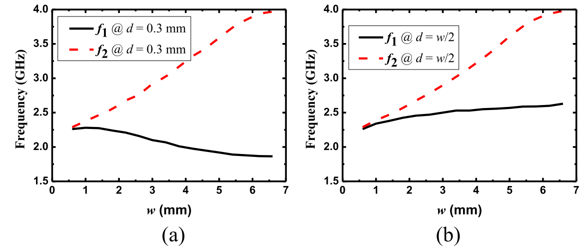

FIGURE 7. Two resonant frequencies f_1 and f_2 varying with w under $r = 7$ mm, $r_s = 0.2$ mm, (a) when $d = 0.3$ mm, (b) when $d = w/2$.

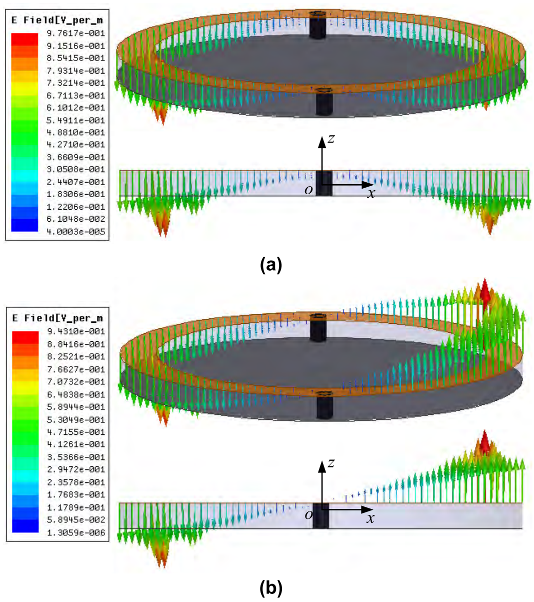

FIGURE 8. Electric field distributions of PLAR. (a) Even mode at f_1, (b) Odd mode (similar to TM_{11} mode of annular ring) at f_2.

As shown in Fig. 7(a), when the shorting pins are placed at a fixed position ($d = 0.3$ mm), f_1 decreases slowly with the increasing of w whereas f_2 increases with a larger slope. As shown in Fig. 7(b), when the shorting pins stay in the middle of annular ring strip ($d = w/2$), both f_1 and f_2 increase, yet with dissimilar slopes. By comparing the red dashed curves in Fig. 7(a) and (b), we can notice that they are almost identical, which means that the positions of shorting pins hardly affect f_2 since f_2 is solely determined by the dimension of the annular ring resonator. Besides, the red and black curves get convergent as illustrated in both Fig. 7(a) and (b) when w and d become small. To be more specific, when $d = 0.3$ mm and $w = 0.6$ mm, $f_1 = 2.261$ GHz and $f_2 = 2.288$ GHz are attained.

The electric field distributions of PLAR for these two resonant modes are displayed in Fig. 8. For the even mode operating at f_1 as shown in Fig. 8(a), two electrical nulls are introduced by shoring pins, and the electric field vectors pointing to the same direction are symmetric with respect to yoz plane. While for the odd mode at f_2, the electric field vectors point to opposite directions along z axis as shown in Fig. 8(b).

B. MODIFIED PLAR ANTENNA IN MUSCLE

It is commonly known that the loading of shorting pins brings extra inductance, which is relatively small in air, therefore causing little frequency separation between f_1 and f_2. When the antenna is embedded in muscle tissue with high permittivity and conductivity ($\varepsilon_r = 52.7$ and $\sigma = 1.74$ S/m at 2.45 GHz), however, the inductance introduced by shorting pins arouses larger influence than it does in air for the first mode, resulting in an even lowered f_1 and therefore enlarged frequency separation. On the other hand, as stated in [30], the TM_{11} mode of annular ring is poor at radiation since the equivalent magnetic current sources of inner and outer ring edges are of opposite polarity and are electrically nearby to each other. In order to reduce the radiation cancellation from the inner and outer ring edges, wide ring width w should be chosen, yielding even higher resonant frequency (f_2) of second mode. Considering the two factors mentioned above, these two resonant frequencies of PLAR antenna in muscle will be separated apart accordingly. However, to obtain wide impedance bandwidth, the first priority is to place these two resonances close to each other, therefore further modification of antenna structure is needed.

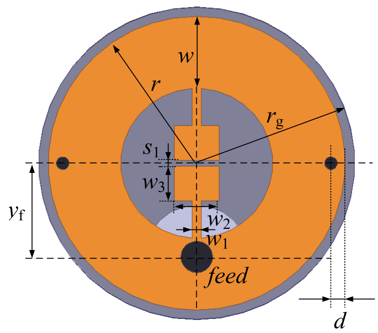

FIGURE 9. Configuration of modified PLAR.

As depicted in Fig. 9, two rectangular patches are introduced and connected to the inner edge of annular ring with high impedance line. The modified PLAR antenna is fed by a coaxial cable of 2 mm long, which is set according to the length of SMA exposed in tissue during measurement. For direct display of frequency shift caused by the introduction of rectangular patch, Fig. 10 compares the $|S_{11}|$ of PLAR before and after modification, and their geometrical parameters are tabulated in Table 1. As shown in Fig. 10, the introduced rectangular patch mainly contributes to the lowering of f_2. With further enlargement of the loaded patch, f_1 and f_2 tend to be merged together, both with linear polarization property.

C. PROPOSED PLAR ANTENNA WITH CP PROPERTY

Similar to the introduction of L-shaped open-end slots discussed in the last section, arc-shaped open-end slots are added to PLAR structure to obtain CP property. The finalized antenna geometry is displayed in Fig. 11 with its detailed geometrical parameters tabulated in Table 2. As shown in Fig. 11,

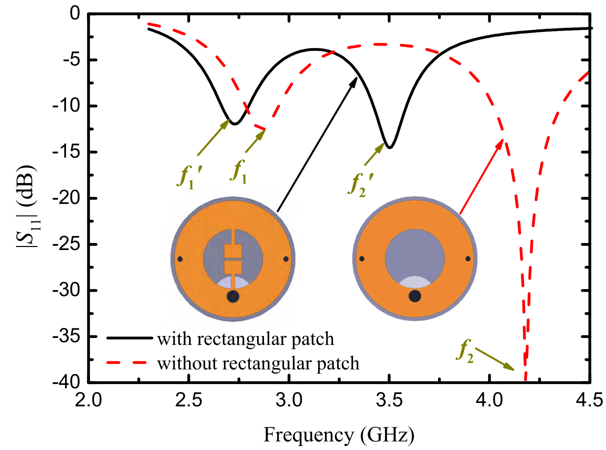

FIGURE 10. $|S_{11}|$ of PLAR with and without rectangular patches loaded.

TABLE 1. Detailed dimensions of modified PLAR antenna (unit: millimeters).

Parameter	Value	Parameter	Value
r_g	5	r	4.7
y_f	3	d	0.4
w	2.3	w_1	0.3
w_2	1.4	w_3	1.1
s_1	0.2		

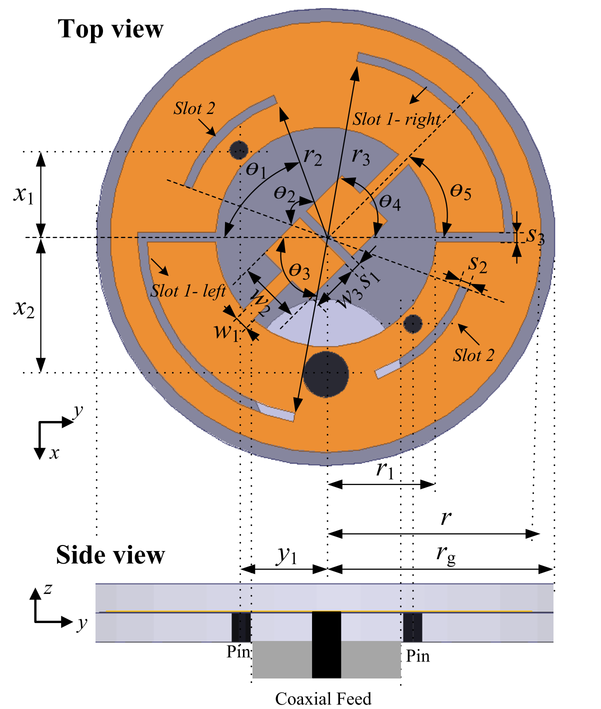

FIGURE 11. Top and side views of PLAR CP antenna with arc-shaped slots.

two sets of slots, symmetric around the center, are inserted in the modified PLAR structure. One set of slots with one end open is a combination of an arc-shaped slot and a rectangular one, labeled as *slot 1*, while another set of arc-shaped slots is labeled as *slot 2*.

TABLE 2. Detailed dimensions of proposed antenna (unit: millimeters).

Parameter	Value	Parameter	Value
r_g	5	r	4.7
r_1	2.4	r_2	3.1
r_3	3.9	x_1	1.9
x_2	3	y_1	1.9
w_1	0.3	w_2	1.4
w_3	1.1	s_1	0.2
s_2	0.2	s_3	0.2
θ_1	70 deg	θ_2	50 deg
θ_3	80 deg	θ_4	80 deg
θ_5	45 deg		

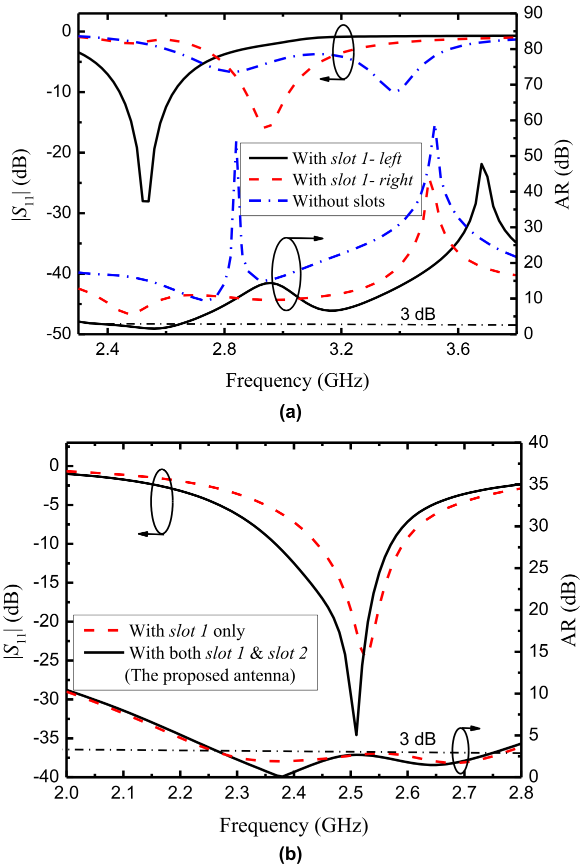

FIGURE 12. Comparison of $|S_{11}|$ and AR for the antenna in Fig. 6 (a) with *slot 1- left*, *slot 1- right* and without slots, (b) with *slot 1* only and with both *slot 1* and *slot 2*.

The comparison of the simulated $|S_{11}|$ and AR at boresight ($\theta = 0$ deg, $\varphi = 0$ deg) between the antennas with and without slots is given in Fig. 7. Fig. 12(a) focuses on the introduction of *slot 1*. It is noted that, for the antenna without any slots, two resonances located at 2.8 and 3.38 GHz can be achieved with linear polarization property. When either part of*slot 1* is inserted, resonances shift to lower bands, indicating further size miniaturization of the antenna. Especially when left part of *slot 1*is introduced, good impedance match appears at 2.52 GHz and AR below 3 dB can be obtained. As a comparison, when right part of *slot 1* is introduced only, good impedance match is achieved at the second mode (2.94 GHz), whereas the impedance match for the first mode (2.48 GHz) is quite poor. Nevertheless, the AR curve still becomes much flatter and its value is much lower (although not below 3 dB) than the *without slots* case for both these two modes.

After combining left and right parts of *slot 1*, the AR performance of the antenna is significantly improved, as illustrated in Fig. 12(b). From the curve *with slot 1 only*, we can see that an impedance bandwidth of 150 MHz ($|S_{11}| < -10$ dB) is achieved, and the AR bandwidth is increased to 480 MHz. When *slot 2* is added, we can widen its impedance bandwidth to 200 MHz ranging from 2.37 to 2.57 GHz, meanwhile further reducing the overall size of the antenna. Besides, its AR bandwidth of 2.27 to 2.75 GHz remains almost the same, with an even lower AR value. Thus far, it has been revealed that the introduction of two sets of slots can indeed realize the CP performance and enhance the impedance bandwidth.

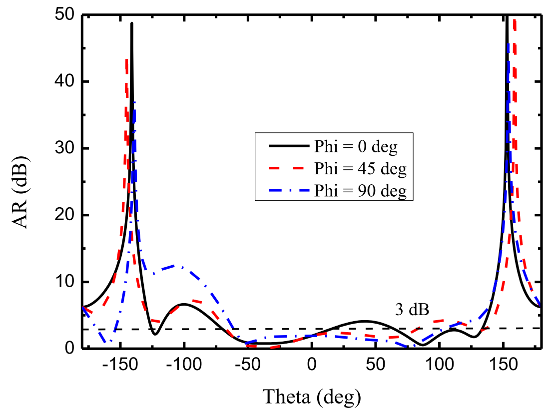

FIGURE 13. Simulated AR beamwidth at 2.45 GHz in three different planes.

Fig. 13 gives the simulated AR beamwidth at 2.45 GHz for proposed antenna in three different planes ($\varphi = 0$, 45 and 90 deg). The presented results show that in $\varphi = 45$ and 90 deg plane, a wide 3-dB AR beamwidth of 145 deg is achieved, ranging from $\theta = -62$ to 83 deg. However, within this θ range, the maximum AR value reaches 4 dB in the plane of $\varphi = 0$ deg. Yet still, a wide 3-dB AR beamwidth of 80 deg, ranging from $\theta = -62$ to 18 deg, can be achieved for all three planes.

Fig. 14 displays the simulated radiation patterns at 2.45 GHz, both in *xoz* and *yoz* planes. The presented results show that RHCP is achieved with a maximum realized gain of -22.7 dBi at boresight, which means the antenna radiates in off-body direction. It should be emphasized herein that the radiation direction is heavily dependent on the loading of human tissue, so the implanted depth is a crucial factor. Particularly, when the antenna is implanted close to the upper surface of human tissue as executed in our design, the main radiation beam points to $+z$ direction. This can be easily understood by the fact that the radiated energy in other

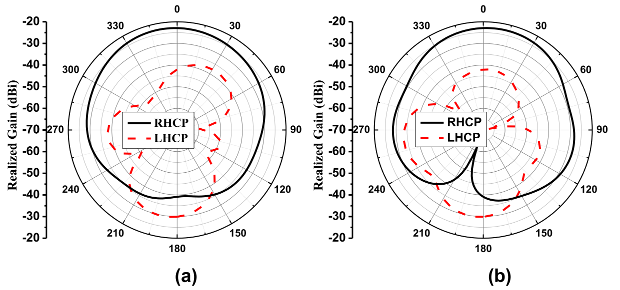

FIGURE 14. Simulated radiation patterns of proposed antenna at 2.45 GHz. (a) at *xoz* plane, (b) at *yoz* plane.

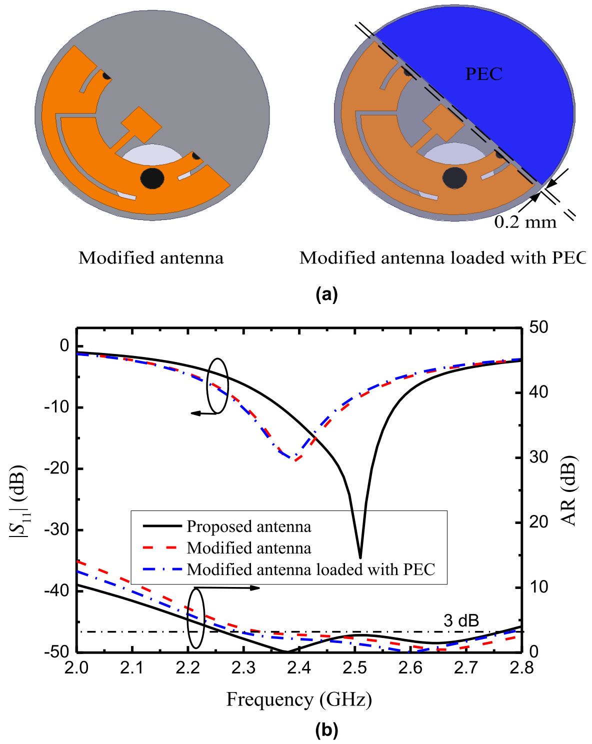

FIGURE 15. (a) Layout of modified antenna with and without PEC loading; (b) Comparison of simulated $|S_{11}|$ and AR before and after modification of the proposed antenna.

directions is tremendously absorbed by lossy tissue around the antenna.

D. MODIFICATION OF THE PROPOSED ANTENNA

Since the proposed PLAR structure is developed from simple pin-loaded patch antenna according to Fig. 6, as long as the loading of slots is maintained, even half of the proposed PLAR can keep its CP property. To verify this phenomenon, a modified antenna is given by cutting the top loaded patch in half as illustrated in the left part of Fig. 15(a). The comparison of simulated results before and after modification reveals that the resonance at f_1 remains, and the AR bandwidth keeps almost unchanged. It indicates that the first mode alone can generate CP waves in our design, while appropriate combination of the two modes leads to impedance bandwidth enhancement with two resonances introduced. In this way, the proposed antenna can be properly modified to reduce its overall size at the expense of impedance bandwidth.

As for the saved space on the top of substrate for the modified structure, it can be used to place other necessary circuits, the influence brought by which needs further evaluation. As depicted in the right part of Fig. 15(a), a semicircular perfect electric conductor (PEC) representing a possible circuit system is placed on the top of substrate, at a distance of 2 mm away from the radiating patch. The simulated $|S_{11}|$ and AR displayed in Fig. 15(b) shows that little influence is caused by the placement of possible circuits.

IV. ANALYSIS AND DISCUSSION

A. PARAMETRIC STUDY OF PROPOSED ANTENNA

For the proposed PLAR antenna, several factors that influence its performance need to be discussed, including the dimension of loaded patches and the length of *slot 1*.

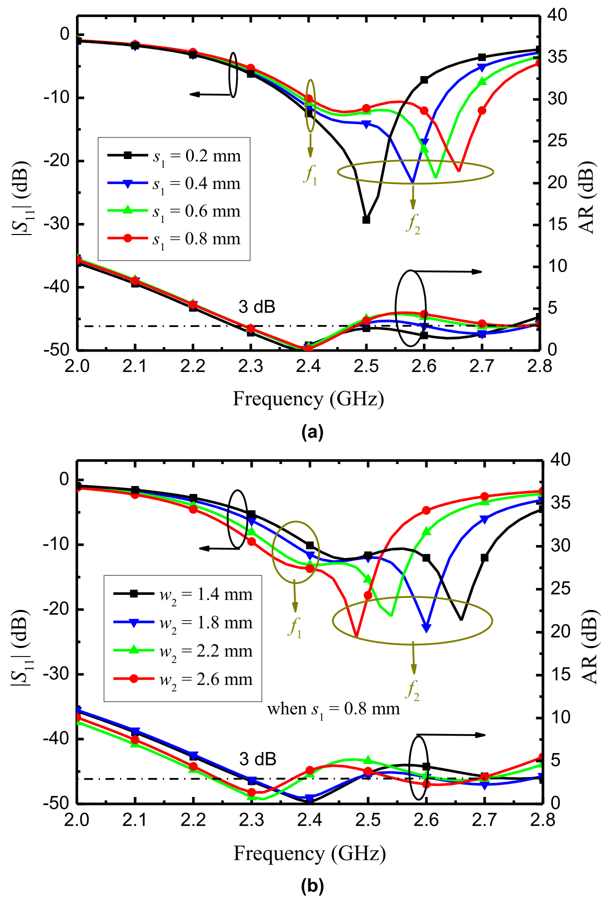

FIGURE 16. Effect of loaded patch dimensions on antenna performance. (a) Effect of s_1. (b) Effect of w_2 when $s_1 = 0.8$ mm.

Fig. 16 illustrates the effect of the dimension of loaded patches on antenna performance. As shown in Fig. 16(a), when the width of central slot s_1 varies from 0.2 to 0.8 mm, the coupling between two patches gets weaker. Simulation results of $|S_{11}|$ show that f_2 moves to higher frequency while f_1 stays unchanged. In correspondence with the $|S_{11}|$ performance, the second notch of simulated AR moves to higher frequency as well, while the first notch stays unchanged.

On the other hand, when the coupling is not sufficiently strong ($s_1 = 0.8$ mm), although we can still keep f_2 close to f_1 for $|S_{11}|$ by adjusting the capacitance between patch and ground plane (increasing w_2), the frequency separation between two notches of AR cannot be reduced. This is largely caused by the fact that both notches move down simultaneously, as shown in Fig. 16(b). In short, strong coupling is highly demanded between two rectangular patches to achieve the expected CP property for the proposed antenna.

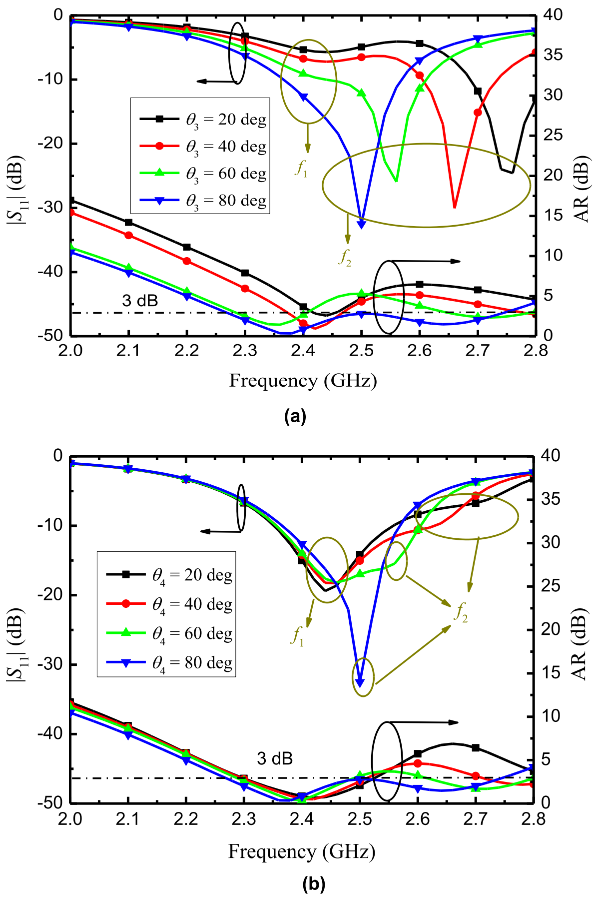

FIGURE 17. Effect of length of *slot 1* on antenna performance. (a) Effect of *slot 1-left*. (b) Effect of *slot 1-right*.

As discussed in Section II-C, the loading of *slot 1* dominates the CP performance of proposed antenna. When different lengths of *slot 1-left* and *slot 1-right* are introduced, different capacitance values can be attained so as to adjust the antenna performance. For *slot 1-left*, we can see from Fig. 17(a) that by changing θ_3, both f_1 and f_2 for $|S_{11}|$ and two notches of AR are largely affected. However, since f_2 and the second notch of AR can be properly tuned by other geometrical parameters, we mainly use θ_3 to improve the impedance matching at f_1 and lower the AR value of the first notch, as already illustrated in Fig. 7(a). As for *slot 1-right*, its length mainly affects the second resonance, which is validated in Fig. 17(b). As θ_4 increases from 20 to 80 deg, f_1 stays almost unchanged while f_2 decreases rapidly from 2.7 to 2.5 GHz. In addition, the second notch of AR is also reduced, thus forming a wide AR bandwidth based on an optimized θ_3.

B. EVALUATION OF STABILITY OF ANTENNA PERFORMANCE

The results of the antenna performance discussed above are all under the condition that an embedded depth $h = 3$ mm is assumed. The antenna performance varied with embedded depth is further studied as shown in Fig. 18. It can be noted herein that $|S_{11}|$ stays almost unchanged as h is enlarged, but the AR value is pushed up to a maximum value of 7 dB in the required band when h equals 12 mm. This deterioration of AR is caused by the dropping of quality factor as embedded depth h gets deepened within high-loss human tissue [31]. Thus, re-optimization of the entire antenna structure needs to be executed, for instance, the perturbation element can be further adjusted to maintain good CP property over a wide operating band.

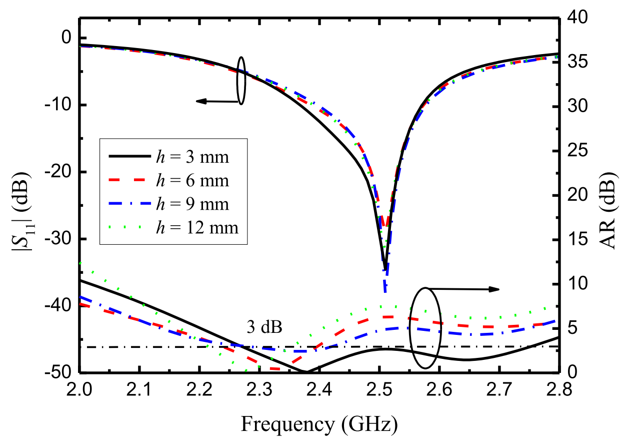

FIGURE 18. Effect of implanted depth *h* on $|S_{11}|$ & AR of proposed antenna.

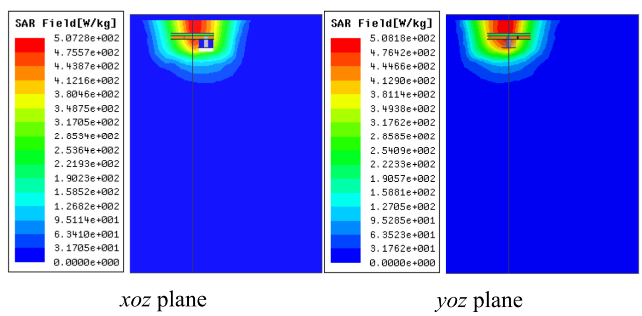

FIGURE 19. Simulated average SAR distribution of proposed antenna in *xoz* and *yoz* planes.

C. SPECIFIC ABSORPTION RATE (SAR) EVALUATION

Due to usual concern on human safety, SAR is evaluated herein in both *xoz* and *yoz* planes. As depicted in Fig. 19, when the input power is set as 1 W, the maximum simulated 1-g average SAR value is 508 W/kg at 2.45 GHz. To effectively protect human from harmful electromagnetic exposure, the allowed input power of the proposed antenna should be less than 3.15 mW, according to IEEE standard [32]. This allowed power is quite enough for most applications. For instance, for wireless neural signal recording application [33], the maximum output power for the transmitter chip is −19 dBm (0.0126 mW), much smaller than the maximum allowed power restricted by SAR.

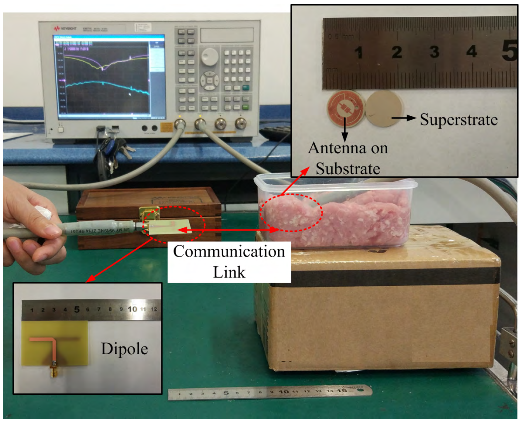

FIGURE 20. Measurement setup together with fabricated antenna.

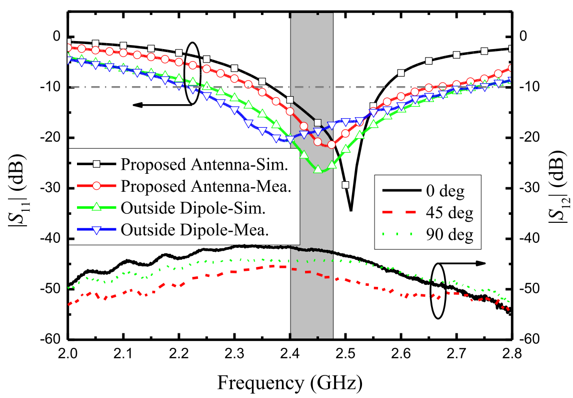

FIGURE 21. Simulated and measured $|S_{11}|$ of proposed antenna and dipole, and $|S_{12}|$ at a distance of 10 mm with rotated angles of 0, 45 and 90 deg.

V. ANTENNA MEASUREMENT

To validate the antenna performances discussed above, the proposed antenna is fabricated and measured in muscle tissue as displayed in Fig. 20. During measurement, a plastic box filled with minced pork is adopted as a substitute of the muscle box in simulation, and the fabricated antenna is embedded in it. Outside the muscle box in air environment, a double-sided dipole resonating at 2.45 GHz is used as an external receiving antenna to establish a wireless link with the implantable antenna. Simulated and measured S-parameters of this link are plotted in Fig. 21, from which we can see that measured result coincides well with simulated one, and a bandwidth of 12.4% (2.34 to 2.65 GHz) is gained. In spite of a little frequency shift, the required 2.45 GHz ISM band is still well covered as indicated in gray.

To testify the CP property exhibited above, $|S_{12}|$ with the external dipole rotated by 0, 45 and 90 deg at a distance of 10 cm is also presented in Fig. 21. It can be seen herein that a maximum difference of 5 dB appears between the coupling strength at all the three planes in the operating band and the strongest coupling attains -41 dB. Furthermore, the $|S_{12}|$ varying with coupling distance from 5 to 20 cm is then measured in these three planes, and the measured results are displayed in Fig. 22, where a maximum difference of 5 dB can be observed as before. Visible discrepancy between the simulation and measurement mainly comes from the influence of the feeding cable and poor accuracy in setting the implanted depth. Finally, the proposed antenna is compared with other previous works in terms of critical parameters, as displayed in Table 3, where all of them operate at 2.45 GHz ISM band. As can be found from Table 3, the proposed antenna has achieved both wide AR bandwidth and compact size. Although the work in [25] has a wider AR bandwidth than this work, its profile is much higher than this work.

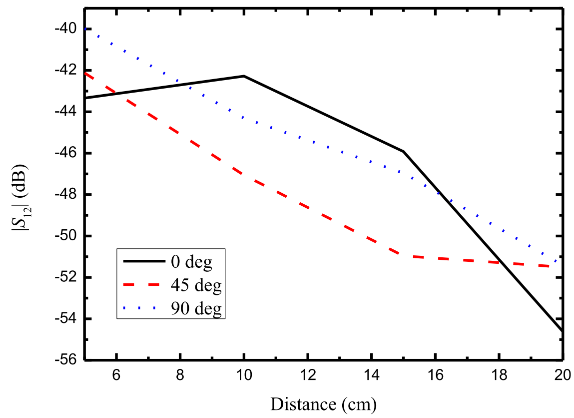

FIGURE 22. Measured coupling strength at varied distances with external dipole under rotated angles of 0, 45 and 90 deg.

TABLE 3. Comparisons between previous works and this work.

Ref.	Implant Depth	Volume (mm^3)	$\|S_{11}\| < -10$ dB	AR < 3 dB
[1]	5 mm	127 (10 × 10 × 1.27)	16.1%	6.1%
[20]	2 mm	91.7 (8.5 × 8.5 × 1.27)	12.2%	2.4%
[21]	4 mm	120.7 ($\pi \times 5.5^2 \times 1.27$)	8.3%	2.49%
[22]	4 mm	127 (10 × 10 × 1.27)	7.7%	1.6%
[25]	50 mm	361.2 ($\pi \times 5.5^2 \times 3.81$)	40%	33.3%
[28]	4 mm	127 (10 × 10 × 1.27)	6.2%	8.13%
This work	3 mm	99.7 ($\pi \times 5^2 \times 1.27$)	8%	19.1%

VI. CONCLUSION

In this paper, a novel wideband implantable CP antenna with a compact size of $\pi \times 5^2 \times 1.27$ $mm^3$is presented for biomedical applications. It is initially developed from a simple patch antenna, whose CP performance is formed by the introduction of shorting pins and L-shaped open-end slot. Then, patch-loaded PLAR structure is adopted as a modification to generate two closely-spaced resonances.

Meanwhile, L-shaped open-end slot is changed to arc-shaped open-end slots to achieve good CP performance. Additionally, extensive parametric studies are conducted. It proves that on one hand, *slot 1-left* dominates the improvement of impedance matching at f_1 and lowers the AR value within the whole band. On the other hand, the central slot between coupling patches and*slot 1-right* mainly affect the second resonance. Finally, antenna performances are measured to validate the simulated ones. Good agreement between them reveals that the proposed implantable antenna has achieved good CP performance with wide AR bandwidth, compact size and good impedance matching.

REFERENCES

[1] J. Kim and Y. Rahmat-Samii, ''Implanted antennas inside a human body: Simulations, designs, and characterizations,'' *IEEE Trans. Microw. Theory Techn.*, vol. 52, no. 8, pp. 1934–1943, Aug. 2004.
[2] T. Karacolak, A. Z. Hood, and E. Topsakal, ''Design of a dual-band implantable antenna and development of skin mimicking gels for continuous glucose monitoring,'' *IEEE Trans. Microw. Theory Techn.*, vol. 56, no. 4, pp. 1001–1008, Apr. 2008.
[3] C.-M. Lee, T.-C. Yo, F.-J. Huang, and C.-H. Luo, ''Dual-resonant Π-shape with double L-strips PIFA for implantable biotelemetry,'' *Electron. Lett.*, vol. 44, no. 14, pp. 837–838, Feb. 2008.
[4] R. Warty, M.-R. Tofighi, U. Kawoos, and A. Rosen, ''Characterization of implantable antennas for intracranial pressure monitoring: Reflection by and transmission through a scalp phantom,'' *IEEE Trans. Microw. Theory Techn.*, vol. 56, no. 10, pp. 2366–2376, Oct. 2008.
[5] P. Soontornpipit, C. M. Furse, and Y. C. Chung, ''Design of implantable microstrip antenna for communication with medical implants,'' *IEEE Trans. Microw. Theory Techn.*, vol. 52, no. 8, pp. 1944–1951, Aug. 2004.
[6] P. M. Izdebski, H. Rajagopalan, and Y. Rahmat-Samii, ''Conformal ingestible capsule antenna: A novel chandelier meandered design,'' *IEEE Trans. Antennas Propag.*, vol. 57, no. 4, pp. 900–909, Apr. 2009.
[7] K. Gosalia, M. S. Humayun, and G. Lazzi, ''Impedance matching and implementation of planar space-filling dipoles as intraocular implanted antennas in a retinal prosthesis,'' *IEEE Trans. Antennas Propag.*, vol. 53, no. 8, pp. 2365–2373, Aug. 2005.
[8] W. Xia, K. Saito, M. Takahashi, and K. Ito, ''Performances of an implanted cavity slot antenna embedded in the human arm,'' *IEEE Trans. Antennas Propag.*, vol. 57, no. 4, pp. 894–899, Apr. 2009.
[9] T. Yilmaz, T. Karacolak, and E. Topsakal, ''Characterization and testing of a skin mimicking material for implantable antennas operating at ISM band (2.4 GHz-2.48 GHz),'' *IEEE Antennas Wireless Propag. Lett.*, vol. 7, pp. 418–420, 2008.
[10] F. Merli, B. Fuchs, J. R. Mosig, and A. K. Skrivervik, ''The effect of insulating layers on the performance of implanted antennas,'' *IEEE Trans. Antenna Propag.*, vol. 59, no. 1, pp. 21–31, Jan. 2011.
[11] A. Kiourti and K. S. Nikita, ''A review of implantable patch antennas for biomedical telemetry: Challenges and solutions,'' *IEEE Antennas Propag. Mag.*, vol. 54, no. 3, pp. 210–228, Jun. 2012.
[12] Z. Duan, Y.-X. Guo, M. Je, and D.-L. Kwong, ''Design and *in vitro* test of a differentially fed dual-band implantable antenna operating at MICS and ISM bands,'' *IEEE Trans. Antennas Propag.*, vol. 62, no. 5, pp. 2430–2439, May 2014.
[13] Z. Duan, L.-J. Xu, S. Gao, and W. Geyi, ''Integrated design of wideband omnidirectional antenna and electronic components for wireless capsule endoscopy systems,'' *IEEE Access*, vol. 6, pp. 29626–29636, 2018.
[14] C. Liu, Y.-X. Guo, and S. Xiao, ''Compact dual-band antenna for implantable devices,'' *IEEE Antennas Wireless Propag. Lett.*, vol. 11, pp. 1508–1511, 2012.
[15] L.-J. Xu, Y.-X. Guo, and W. Wu, ''Dual-band implantable antenna with open-end slots on ground,'' *IEEE Antennas Wireless Propag. Lett.*, vol. 11, pp. 1564–1567, 2012.
[16] A. Kiourti and K. S. Nikita, ''Miniature scalp-implantable antennas for telemetry in the MICS and ISM bands: Design, safety considerations and link budget analysis,'' *IEEE Trans. Antennas Propag.*, vol. 60, no. 8, pp. 3568–3575, Aug. 2012.
[17] Y. Liu, Y. Chen, H. Lin, and F. H. Juwono, ''A novel differentially fed compact dual-band implantable antenna for biotelemetry applications,'' *IEEE Antennas Wireless Propag. Lett.*, vol. 15, pp. 1791–1794, 2016.
[18] Y. H. Jung *et al.*, ''A compact parylene-coated WLAN flexible antenna for implantable electronics,'' *IEEE Antennas Wireless Propag. Lett.*, vol. 15, pp. 1382–1385, 2016.
[19] H. Li, Y.-X. Guo, and S.-Q. Xiao, ''Broadband circularly polarised implantable antenna for biomedical applications,'' *Electron. Lett.*, vol. 52, no. 7, pp. 504–506, Mar. 2016.
[20] X. Y. Liu, Z. T. Wu, Y. Fan, and E. M. Tentzeris, ''A miniaturized CSRR loaded wide-beamwidth circularly polarized implantable antenna for subcutaneous real-time glucose monitoring,'' *IEEE Antennas Wireless Propag. Lett.*, vol. 16, pp. 577–580, 2016.
[21] R. Li, Y.-X. Guo, B. Zhang, and G. Du, ''A miniaturized circularly polarized implantable annular-ring antenna,'' *IEEE Antennas Wireless Propag. Lett.*, vol. 16, pp. 2566–2569, 2017.
[22] C. Liu, Y.-X. Guo, and S. Xiao, ''Capacitively loaded circularly polarized implantable patch antenna for ISM band biomedical applications,'' *IEEE Trans. Antennas Propag.*, vol. 62, no. 5, pp. 2407–2417, May 2014.
[23] K. Zhang, C. Liu, X. Liu, H. Guo, and X. Yang, ''Miniaturized circularly polarized implantable antenna for ISM-band biomedical devices,'' *Int. J. Antennas Propag.*, Mar. 2017, Art. no. 9750257.
[24] C. Liu, Y. Zhang, and X. Liu, ''Circularly polarized implantable antenna for 915 MHz ISM-band far-field wireless power transmission,'' *IEEE Antennas Wireless Propag. Lett.*, vol. 17, no. 3, pp. 373–376, Mar. 2018.
[25] C. Liu, Y.-X. Guo, and S. Xiao, ''Circularly polarized helical antenna for ISM-band ingestible capsule endoscope systems,'' *IEEE Trans. Antennas Propag.*, vol. 62, no. 12, pp. 6027–6039, Dec. 2014.
[26] Z. Duan and L.-J. Xu, ''Dual-band implantable antenna with circular polarisation property for ingestible capsule application,'' *Electron. Lett.*, vol. 53, no. 16, pp. 1090–1092, Aug. 2017.
[27] L.-J. Xu, Y.-X. Guo, and W. Wu, ''Miniaturized circularly polarized loop antenna for biomedical applications,'' *IEEE Trans. Antennas Propag.*, vol. 63, no. 3, pp. 922–930, Mar. 2015.
[28] Z.-J. Yang, S.-Q. Xiao, L. Zhu, B.-Z. Wang, and H.-L. Tu, ''A circularly polarized implantable antenna for 2.4-GHz ISM band biomedical applications,'' *IEEE Antennas Wireless Propag. Lett.*, vol. 16, pp. 2554–2557, 2017.
[29] I. J. Bahl, S. S. Stuchly, and M. A. Stuchly, ''A new microstrip radiator for medical applications,'' *IEEE Trans. Microw. Theory Techn.*, vol. MTT-28, no. 12, pp. 1464–1469, Dec. 1980.
[30] W. Chew, ''A broad-band annular-ring microstrip antenna,'' *IEEE Trans. Antennas Propag.*, vol. AP-30, no. 5, pp. 918–922, Sep. 1982.
[31] Z.-J. Yang, L. Zhu, and S. Xiao, ''An implantable circularly polarized patch antenna design for pacemaker monitoring based on quality factor analysis,'' *IEEE Trans. Antennas Propag.*, vol. 66, no. 10, pp. 5180–5192, Oct. 2018.
[32] *IEEE Standard for Safety Levels With Respect to Human Exposure to Radio Frequency Electromagnetic Fields, 3 KHz to 300 GHz*, IEEE Standard C95.1-1999, 1999.
[33] Z. M. Chen, K.-W. Cheng, Y. Zheng, and M. Je, ''A 3.4-mW 54.24-Mbps burst-mode injection-locked CMOS FSK transmitter,'' in *Proc. IEEE Asian Solid-State Circuits Conf.*, Nov. 2011, pp. 289–292.

LI-JIE XU received the B.E. degree in optoelectronic information and engineering and the Ph.D. degree in electromagnetic field and microwave technology from the Nanjing University of Science and Technology (NUST), in 2009 and 2014, respectively.

From 2010 to 2011, she was a Visiting Scholar with the Department of Electrical and Computer Engineering (ECE), National University of Singapore (NUS). From 2011 to 2013, she was a Joint Ph.D. Student, supported by the China Scholarship Council (CSC), with the Department of ECE, NUS. She is currently an Associate Professor with the College of Electronic and Optical Engineering, Nanjing University of Post and Telecommunications, and holds a postdoctoral position with the School of Information Science and Engineering, Southeast University. Her main research interests include implantable/wearable antennas for biomedical applications, and low-pass and bandpass filters.

YAMING BO (M'97) received the B.Eng. and M.Eng. degrees in radio engineering from the Nanjing Institute of Technology (now Southeast University), Nanjing, China, in 1985 and 1988, respectively, and the Ph.D. degree in engineering from Southeast University, Nanjing, China, in 1992.

He was a Lecturer with the Department of Radio Engineering, Southeast University, from 1992 to 1993. He visited the Department of Electrical Engineering, City University of Hong Kong, from 1993 to 1994. From 1994 to 1996, he was an Associate Professor with the Department of Radio Engineering, Southeast University. From 1996 to 2005, he was an Associate Professor with the Wuxi University of Light Industry (now Jiangnan University), Wuxi, Jiangsu, China. He was the Vice Dean of the School of Communication and Control Engineering and the Postgraduate School, Wuxi University of Light Industry, from 1998 to 2003 and from 2003 to 2005, respectively. As a Visiting Scholar, he visited the Institute of Mobile and Satellite Communication Techniques (IMST), Kamp-Lintfort, Germany, under the support of Alfried Krupp und Bohlen und Halbach Stiftung, from 2000 to 2001. In 2005, he joined the Faculty of Nanjing University of Posts and Telecommunication, Nanjing. From 2008 to 2009, he visited the National University of Singapore, Singapore, as a Research Scientist. He has been a Professor with the School of Communication Engineering, Nanjing University of Posts and Telecommunications, since 2008. He has authored or coauthored over 100 journal and conference papers and is the co-inventor of nine granted Chinese patents. His current research interests include computational electromagnetics, antenna techniques, electromagnetic scattering, and evolutionary optimization algorithms. He was a co-recipient of the Science and Technology Progress Award from the State Education Commission, China, in 1993, and the Scientific and Technological Awards from the Chinese Institute of Communications, China, in 2009.

WEN-JUN LU (M'12) was born in Jiangmen, Guangdong, China, in 1978. He received the Ph.D. degree in electrical engineering from the Nanjing University of Posts and Telecommunications (NUPT), Nanjing, China, in 2007, where he has been a Professor with the Jiangsu Key Laboratory of Wireless Communications, since 2013. He has authored or coauthored over 160 technical papers published in peer-reviewed international journals and conference proceedings. He is the Translator of the Chinese version of *The Art and Science of Ultrawideband Antennas* (by H. Schantz). He has authored *Antennas: Concise Theory, Design and Applications* (in Chinese). His research interests include antenna theory, wideband antennas, and antenna arrays. He has been serving as an Editorial Board Member of the *International Journal of RF and Microwave Computer-Aided Engineering*, since 2014. He was a recipient of the Exceptional Reviewers Award of the IEEE TRANSACTIONS ON ANTENNAS AND PROPAGATION, in 2016.

LEI ZHU (S'91–M'93–SM'00–F'12) received the B.Eng. and M.Eng. degrees in radio engineering from the Nanjing Institute of Technology (now Southeast University), Nanjing, China, in 1985 and 1988, respectively, and the Ph.D. degree in electronic engineering from the University of Electro-Communications, Tokyo, Japan, in 1993.

From 1993 to 1996, he was a Research Engineer with Matsushita-Kotobuki Electronics Industries, Ltd., Tokyo. From 1996 to 2000, he was a Research Fellow with the École Polytechnique de Montréal, Montreal, QC, Canada. From 2000 to 2013, he was an Associate Professor with the School of Electrical and Electronic Engineering, Nanyang Technological University, Singapore. He joined the Faculty of Science and Technology, University of Macau, Macau, China, as a Full Professor, in 2013, where he has been a Distinguished Professor, since 2016. From 2014 to 2017, he served as the Head of Department of Electrical and Computer Engineering, University of Macau. He is currently a Visiting Professor with the Nanjing University of Posts and Telecommunications. So far, he has authored or coauthored more than 490 papers in international journals and conference proceedings. His papers have been cited more than 6100 times with the H-index of 41 (source: ISI Web of Science). His research interests include microwave circuits, guided-wave periodic structures, planar antennas, and computational electromagnetic techniques.

Dr. Zhu served as a member of the IEEE MTT-S Fellow Evaluation Committee, from 2013 to 2015, and the IEEE AP-S Fellows Committee, from 2015 to 2017. He was a recipient of the 1993 First-Order Achievement Award in Science and Technology from the National Education Committee, China, the 1996 Silver Award of Excellent Invention from Matsushita-Kotobuki Electronics Industries, Ltd., and the 1997 Asia–Pacific Microwave Prize Award. He served as the General Chair of the 2008 IEEE MTT-S International Microwave Workshop Series on the Art of Miniaturizing RF and Microwave Passive Components, Chengdu, China, and the Technical Program Committee Co-Chair of the 2009 Asia–Pacific Microwave Conference, Singapore. He was an Associate Editor of the IEEE MICROWAVE AND WIRELESS COMPONENTS LETTERS, from 2006 to 2012 and IEEE TRANSACTIONS ON MICROWAVE THEORY AND TECHNIQUES, from 2010 to 2013.

CHENG-FEI GUO was born in Mianyang, Sichuan, China, in 1997. He is currently pursuing the bachelor's degree with the School of Communication and Information Engineering, Nanjing University of Posts and Telecommunications.

His main research interests include circular polarization, biomedical, and antennas.